Ocean Engineering 62 (2013) 78–90

Contents lists available at SciVerse ScienceDirect

Ocean Engineering

journal homepage: www.elsevier.com/locate/oceaneng

Simple absorbing layer conditions for shallow wave simulations with Smoothed Particle Hydrodynamics

Diego Molteni [a,*], Rosario Grammauta [a], Enrico Vitanza [b]

[a] Dipartimento di Fisica, Viale delle Scienze, Università di Palermo, Italy
[b] Dipartimento di Ingegneria Civile, Ambientale e Aerospaziale, Università di Palermo, Italy

ARTICLE INFO

Article history:
Received 27 February 2012
Accepted 23 December 2012

Keywords:
Fluid mechanics
Boundary condition
Absorbing layer
Lagrangian numerical method
SPH
Shallow water model

ABSTRACT

We study and implement a simple method, based on the Perfectly Matched Layer approach, to treat non reflecting boundary conditions with the Smoothed Particles Hydrodynamics numerical algorithm. The method is based on the concept of physical damping operating on a fictitious layer added to the computational domain. The method works for both 1D and 2D cases, but here we illustrate it in the case of 1D and 2D time dependent shallow waves propagating in a finite domain.

1. Introduction

The problem of non reflecting boundary conditions is an old subject of the study of wave propagation in limited domains. The so called radiation boundary conditions at infinity have been studied since 1912 by Sommerfeld, but its practical implementation in computational solutions of electromagnetic field propagation can be referred to Engquist and Majda (1977). It is obvious that the occurrence of boundaries affects the evolution of a physical event that would otherwise propagate into open space. Many different strategies have been adopted to circumvent the problem. Among numerous approaches the method of characteristics is well exploited in the fixed grid numerical methods (Poinsot and Lele, 1992). The perfectly matched layer (PML) approach, i.e. the use of an artificial absorbing layer, was devised by Berenger (1994) for simulations of electromagnetic waves and successively adopted in many wave field simulations: acoustics, seismic vibrations and fluids. The general idea of the PML approach is very simple. An absorbing layer is added to the physical domain. In this layer, sink or source terms are activated, multiplied by a coefficient varying from zero, inside the physical domain, to a maximum at the outer edge of the layer zone. The mathematical properties to be attributed to this zone can reach great accuracy and complexity, as shown in the paper by Lin et al. (2011) on recent advancements for non-linear regime of the Euler equations to be adopted in the layer. Recently Modave et al. (2010) set up a simple and accurate PML method that is useful for linear and non-linear shallow water simulations. We essentially adopt this simpler approach.

2. The absorbing layer method

In general, the model equations governing the fluid dynamics are rewritten adding a sink or source term to the original equations, as follows:

$$\frac{\partial A}{\partial t} = f\left(A, \frac{\partial A}{\partial x}, x\right) - \sigma(A - A_{out}) \tag{0.1}$$

where A is a generic fluid variable, $-\sigma(A-A_{out})$ is the corresponding sink or source term, A_{out} is the external boundary value, σ is the damping coefficient different from zero only in the damping region. With an appropriate choice of the σ spatial function this procedure produces extremely small reflection waves.

All these techniques are used for fixed grids discretization of the equations. In the Lagrangian approach the characteristic lines method has been suggested by Lastiwka et al. (2009) and Vacondio et al. (2012) which uses a simplified version of that procedure. Instead the PML approach is by far simpler, but, as far as we know, it has not been studied in the context of a Lagrangian approach. We adopted this strategy for the Lagrangian Smoothed Particle Hydrodynamics scheme and tested it in the case of waves propagating in a finite tank. We show that the results are fairly good.

* Corresponding author. Tel.: +39 091 6615055; fax: +39 091 6615069.
E-mail addresses: diego.molteni@unipa.it, prof.molteni@gmail.com (D. Molteni).

0029-8018/$ - see front matter © 2013 Elsevier Ltd. All rights reserved.
http://dx.doi.org/10.1016/j.oceaneng.2012.12.048

The Smoothed Hydrodynamics method (SPH) is a Lagrangian mesh-free method based on a single basic interpolating function associated with each node of the moving mesh.

Here we give the basic ideas. For an up to date detailed presentation of the SPH method see Colagrossi and Landrini (2003). A function f is interpolated from its known values at points k, by the approximation of the Dirac function integral:

$$f(x) = \int f(y)\delta(x-x')dy \Rightarrow \tilde{f}(x) = \sum_k f_k W(x,x'_k)\Delta x'_k \tag{0.2}$$

where $W(x,x'_k)$ is the interpolating function, named kernel, centered in the x'_k point. This interpolating function has a scale factor h and must have the properties to mimic the Dirac function, therefore

$$\int_{-\infty}^{+\infty} W(x/h)dx = 1 \quad \text{and} \quad \lim_{h\to 0} W(x/h) = \delta(x)$$

and $\tilde{f}(x)$ is the approximated function. Exploiting the mass density ρ, we can attribute to each moving node a mass $m_k = \rho_k \Delta x'_k$ and

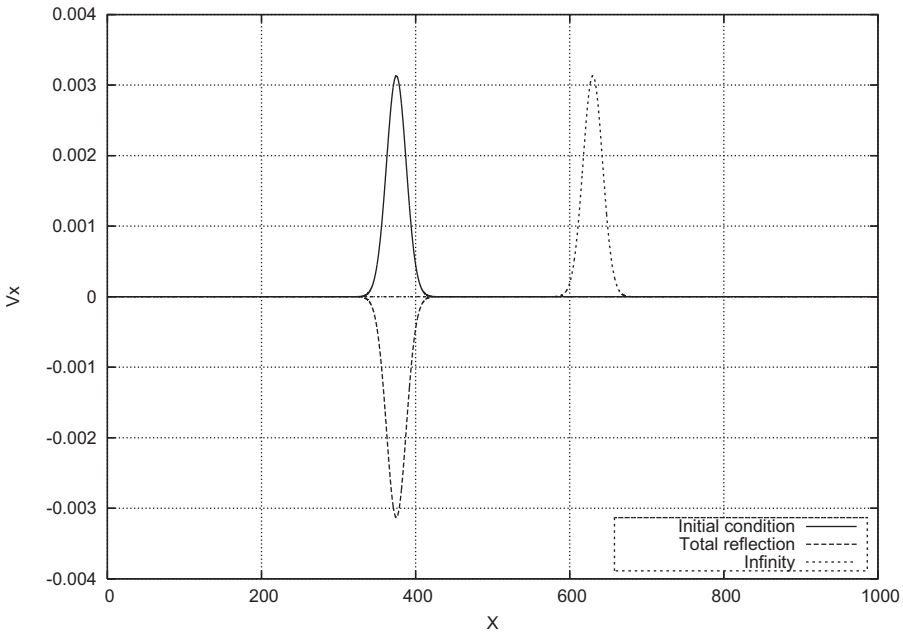

Fig. 1. Initial pulse profile chosen $H_0=1$, $x_c=3/4X$ and $A=9h$ solid line; the perfectly reflected pulse: dashed line and the infinity case: dotted line.

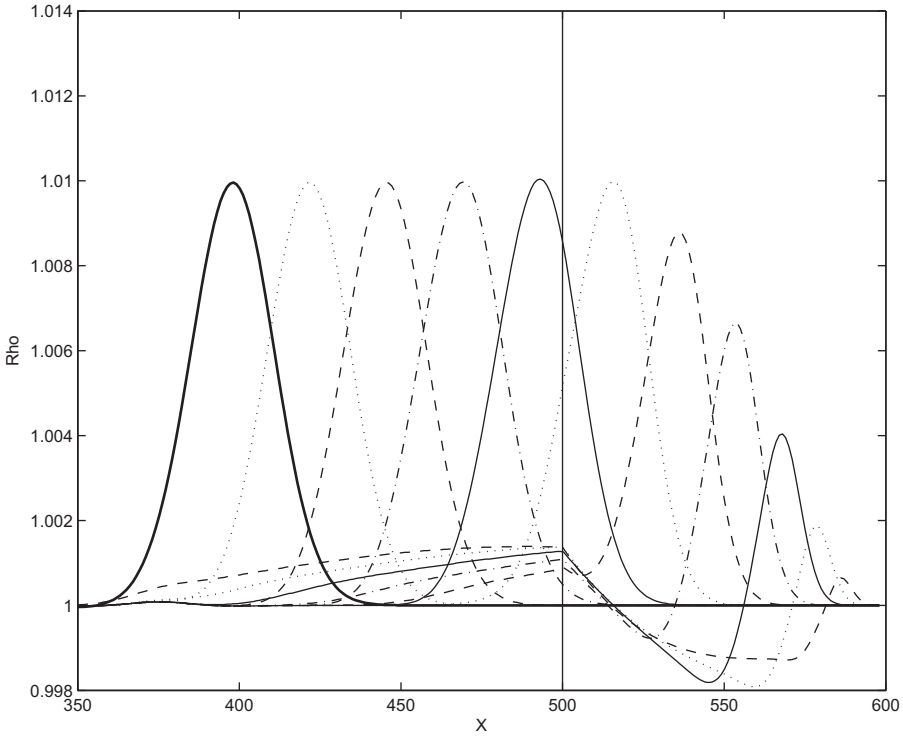

Fig. 2. Time evolution of the wave height at intervals of 7.4 s; the bold solid line represents the initial configuration.

therefore the approximated function is given by

$$\tilde{f}(x)=\sum_k m_k\frac{f_k}{\rho_k}W(x,x'_k) \tag{0.3}$$

Consequently the space derivative can be approximated as

$$\frac{\partial f}{\partial x}\approx\int\frac{\partial f(x')}{\partial x'}W(x-x')dx'\approx\sum_k\frac{m_k}{\rho_k}f_k\frac{\partial W_{ik}}{\partial x_i} \tag{0.4}$$

Many details on the SPH approach can be also found in the review of Monaghan (2005). We give here the final formulae.

The continuity equation is given by

$$\frac{d\rho}{dt}=-\rho\nabla\vec{v}\Rightarrow\frac{d\rho_i}{dt}=\sum_k m_k(\vec{v}_i-\vec{v}_k)\cdot\nabla_i W(\vec{r}_i,\vec{r}_k) \tag{0.5}$$

The momentum equation is

$$\frac{d\vec{v}}{dt}=-\frac{1}{\rho}\nabla P\Rightarrow\frac{d\vec{v}_i}{dt}=-\sum_k m_k\left(\frac{P_i}{\rho_i^2}+\frac{P_k}{\rho_k^2}+\Pi_{ik}\right)\nabla_i W(\vec{r}_i,\vec{r}_k) \tag{0.6}$$

P is the pressure to be given by an equation of state specific to the problem to be studied, that will be specified in the subsections. Π_{ik} is an artificial viscosity term needed to stabilize the equations (cfr. Monaghan, 2005) and $W(\vec{r}_i,\vec{r})$ is the interpolating function, named kernel, centered in the $\vec{r}_i$ point. This interpolating function has a scale factor h and must have the properties to mimic the Dirac function, therefore

$$\int_{-\infty}^{+\infty}W(r/h)d^n x=1\quad\text{and}\quad\lim_{h\to 0}W(r/h)=\delta(r)$$

The kernel used for our 2D simulation is the Wendland kernel function, where n is the spatial dimension

$$W(r,h)=\frac{7}{4\pi h^n}\begin{cases}\left(1-\frac{r}{2h}\right)^4\left(1+2\frac{r}{h}\right) & \text{if } \frac{r}{h}\le 2\\ 0 & \text{if } \frac{r}{h}>0\end{cases} \tag{0.7}$$

The integration in time is carried out by the predictor corrector algorithm for low Mach number flows, accurate to second order in the time step, proposed by Monaghan (2006). The time step is limited by the usual Courant condition.

3. Lagrangian formulation of shallow water equations

We focus our attention to the open boundaries problem for the shallow water waves in the SPH framework. The general gravity wave case has been accurately studied, but not in the context of boundary problems, by Antuono et al. (2011). The governing equations, in conservative Eulerian form, for shallow water waves, derived under the usual approximations of wave elevation much smaller than the full water depth and for constant bottom elevation, are well known:

$$\frac{\partial H}{\partial t}+div(H\vec{v})=0 \tag{0.8}$$

$$\frac{\partial H\vec{v}}{\partial t}+div\left(H\vec{v}\otimes\vec{v}+g\frac{H^2}{2}\mathbf{I}\right)=0 \tag{0.9}$$

where H is the full height of the water level, g is the gravitational acceleration, and $\vec{v}$ is the fluid velocity.

De Leffe et al. (2010) also derived an SPH formulation slightly different from the one presented in this paper.

3.1. The 1D shallow water case

To outline important physical elements in the absorbing zone we begin to analyze the simple 1D case. When written in the Lagrangian form, we have for the wave height equation

$$\frac{dH}{dt}=-H\frac{\partial v}{\partial x} \tag{0.10}$$

where $d\ldots/dt$ is the comoving derivative. The equation of motion is

$$\frac{dv}{dt}=-g\frac{\partial H}{\partial x} \tag{0.11}$$

These equations can be formally satisfied by a *fictitious* fluid having a density $\rho=H$ and an equation of state for the pressure $P=(1/2)g\rho^2$, so that the shallow water equations are fulfilled by this *special fluid* and therefore can be immediately approximated by the standard SPH formulae. Then the SPH shallow wave

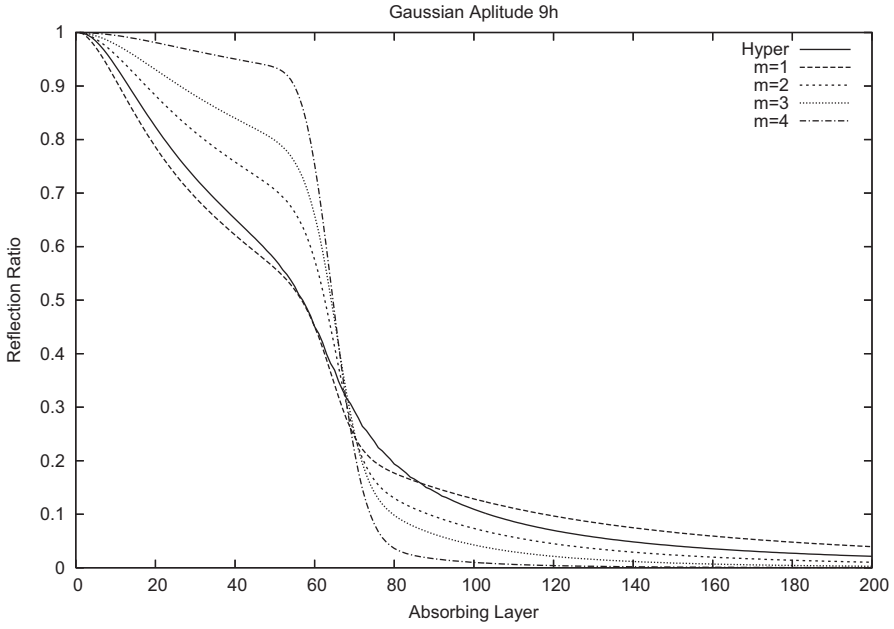

Fig. 3. Reflection ratio versus the thickness of the absorbing layer for σ function, hyperbolic and power law function with different values of the exponent m. The parameters are identical to those used in Fig. 1.

equations are

$$\frac{dH}{dt} = -H\nabla\vec{v} \Rightarrow \frac{dH_i}{dt} = \sum_k m_k(\vec{v}_i - \vec{v}_k)\cdot\nabla_i W(\vec{r}_i, \vec{r}_k) \tag{0.12}$$

where $m_k = H\Delta x_k$. For the momentum equation we adopted a slightly different formulation that produces more accurate results due to its higher sensitivity to the pressure gradient for this peculiar equation of state. This equation has been used for instance by Riadh and Azzedine (2005) in their study of shallow water flows with SPH:

$$\frac{d\vec{v}}{dt} = -\frac{1}{\rho}\nabla P \Rightarrow \frac{d\vec{v}_i}{dt} = -\sum_k m_k\left(\frac{P_i+P_j}{\rho_i\rho_j} + \Pi_{ik}\right)\nabla_i W(\vec{r}_i, \vec{r}_k)$$

Since $P=(1/2)g\rho^2$ and $\rho \equiv H$, then for shallow water momentum equation we have

$$\frac{d\vec{v}_i}{dt} = -\sum_k m_k\left(\frac{1}{2}g\frac{H_i^2+H_j^2}{H_iH_j} + \Pi_{ik}\right)\nabla_i W(\vec{r}_i, \vec{r}_k) \tag{0.13}$$

3.2. Test description and damping technique

In a domain of amplitude $X=500$ we produce a Gaussian pulse in the density profile and a corresponding fluid speed according to the following prescription:

$$H(x) = H_0\left(1 + 0.01\exp\left(-\frac{(x-x_c)^2}{A^2}\right)\right) \tag{0.14}$$

$$v(x) = (H(x)-H_0)\sqrt{gH_0} \tag{0.15}$$

So we have a 1D soliton traveling towards the right side of the domain. The following pulse parameters have been chosen $H_0=1$, $x_c=3/4X$ and $A=9h$. The interpolating particle size is $h=2$, and the particle spacing is $\Delta x=1$. All quantities are in SI units.

A physical damping can, obviously, produces attenuation of outgoing signals; however, Fourier analysis shows that not all the harmonics belonging to a signal are attenuated and a special shape of the damping is needed, as developed for example by Modave et al. (2010) who made a good mathematical analysis that can be assumed to be valid also for the Lagrangian SPH method at least in the shallow waves case, since the fluid speed is very small (essentially no mass transport) compared to the wave speed.

To damp appropriately the waves in proximity of the domain edge an extra spatial layer is added to the domain and the equations in this damping layer are

$$\frac{dH}{dt} = -H\frac{\partial v}{\partial x} - \sigma(x)(H-H_0) \tag{0.16}$$

for the water level, and

$$\frac{dv}{dt} = -g\frac{\partial H}{\partial x} - \sigma(x)(v-v_0) \tag{0.17}$$

for the speed of the fluid,

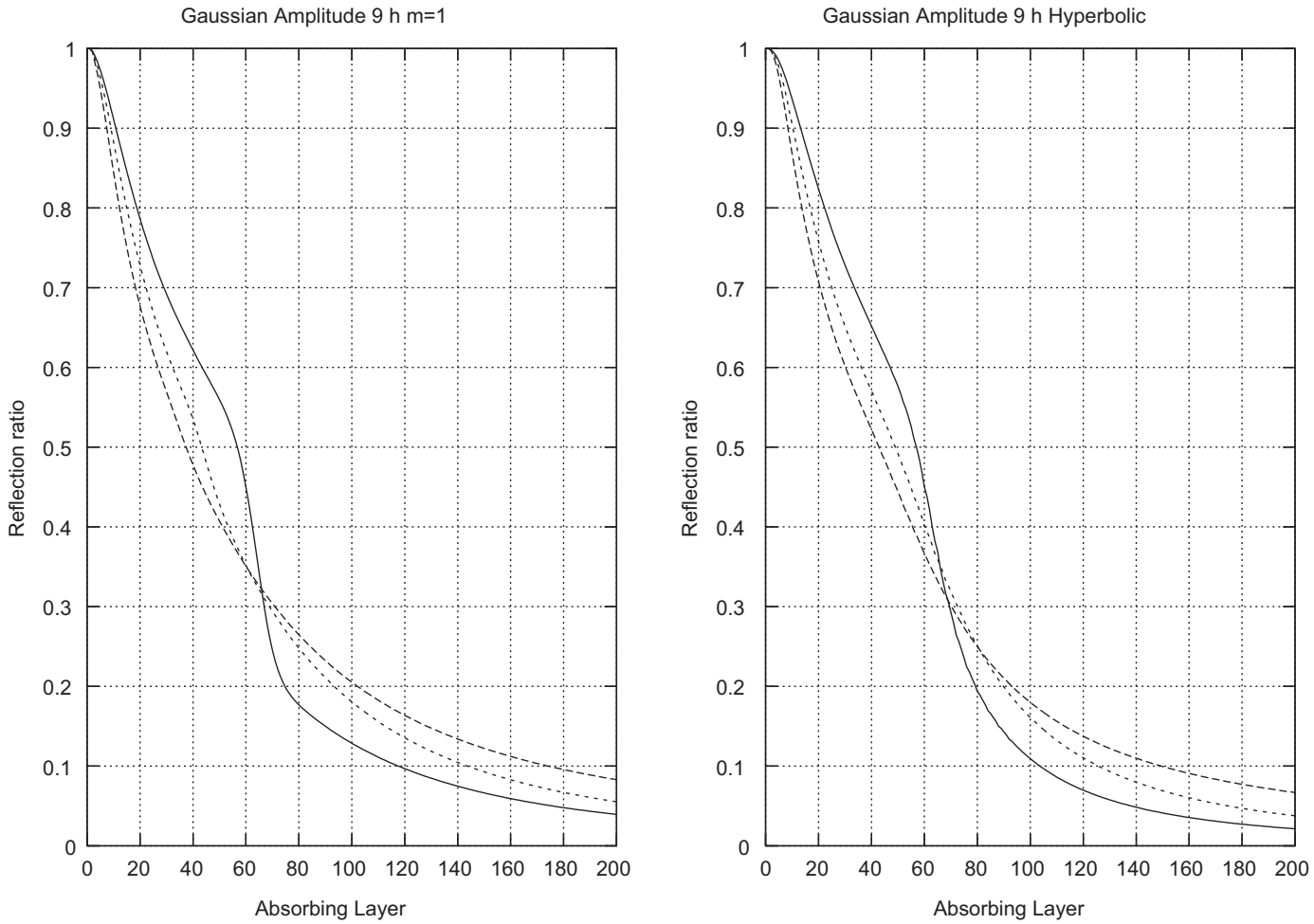

Fig. 4. Reflection versus the thickness of the absorbing layer for two different absorbing coefficient functions (left panel: $m=1$, right panel: hyperbolic). The solid line identifies the case with the use of only the clean function, and the dashed line identifies clean function multiplied by f_1. The dotted line identifies the clean function multiplied by f_2. The parameters are identical to those used in Fig. 1.

where $\sigma(x)$ is the damping coefficient, which is a function of the position in the layer, having an appropriate spatial dependence (discussed below); and v_0 is the outflow speed. In our study we impose $v_0=0$ since in our case waves are propagating in a closed water tank.

To produce a damping layer we add the following terms:

1. $S=-\sigma(x)(H-H_0)$ to the density equation.
2. $Q=-\sigma(x)(v-v_0)$ to the momentum equation.

We tested for the coefficient σ the following functions suggested by Modave et al. (2010): $\sigma=\sigma_0[(x-x_0)/L]^m$ where m is a positive integer, and $\sigma=\sigma_0[(x-x_0)/((x_0+L)-x)]$ where x_0 is the starting point of the absorbing zone. L is the thickness of the zone and m is an exponent to be tuned.

Furthermore we tested also two ad *hoc* treatments, we call them *switches*, based on physical intuition:

a. decrease the horizontal pressure force, only in the damping layer, with particular functions f_1 or f_2.

$$f_1(x)=\begin{cases} -\frac{x-(x_0+L)}{L} & x_0<x<x_0+L \\ 1 & x\le x_0 \end{cases}$$

$$f_2(x)=\begin{cases} \frac{L^2-(x-x_0)^2}{L^2} & x_0<x<x_0+L \\ 1 & x\le x_0 \end{cases}$$

f_1 is a linear function, f_2 is a parabolic function with its maximum at x_0. The forces on the particles are simply multiplied by these functions. We call them, *cutting functions* since they reduce to zero the horizontal force acting on particles close to the end of the damping layer. In this case the basic physical idea is to decrease smoothly the pressure gradient near the boundary.

b. Use the damping friction $\sigma>0$ only if $v_x<0$. In this case the idea is to damp preferentially fluid motion directed into the domain.

Fig. 1 shows the initial analytical configuration for the fluid speed V_x (not the wave speed) and both the totally reflected Gaussian and the undisturbed propagated wave (we call it *infinity case*) both computed at the time $t=((X/2)/(\sqrt{gH_0}))$. By "*infinity*" we mean the remnant of the numerical solution in the computational domain when the corresponding peak of the analytical solution went out of the integration domain. It is obtained by simply integrating the numerical solution into a much larger numerical domain, obviously consuming more CPU time.

The total reflection profile is due to the wave coming back at the perfectly rigid boundary located at the right domain edge $X=500$ m. The reflection ratio R for this set of 1D simulations is

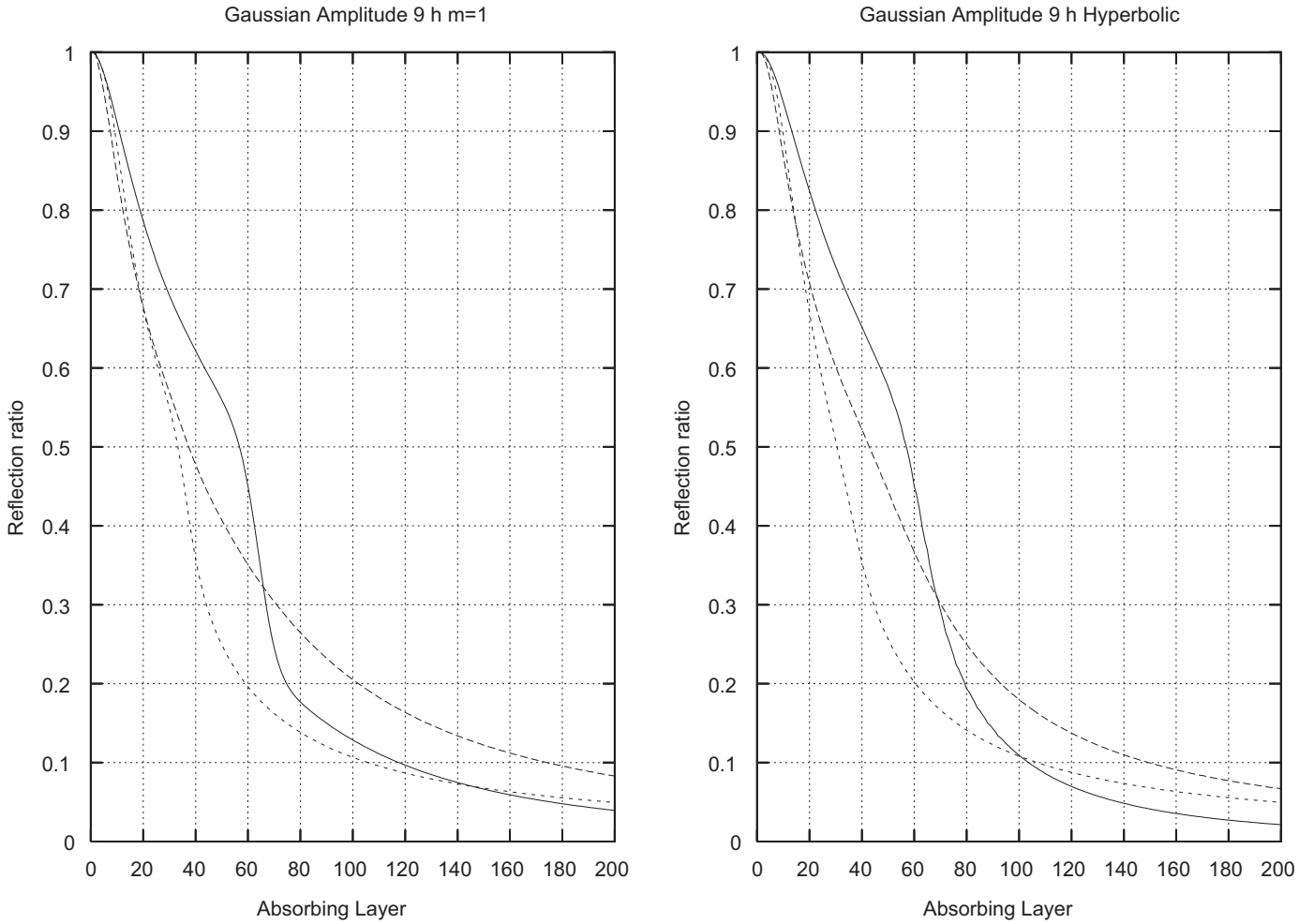

Fig. 5. Reflection ratio versus the thickness of the absorbing layer for two different distributions of the absorption coefficient (left panel: $m=1$, right panel: hyperbolic). The solid line identifies the case with the use of the clean function, and the dashed line identifies the same case with the attenuation of the force added with a linear function f_1 within the layer zone. The dotted line identifies the previous case with a further switch on the speed. The parameters are identical to those used in Fig. 1.

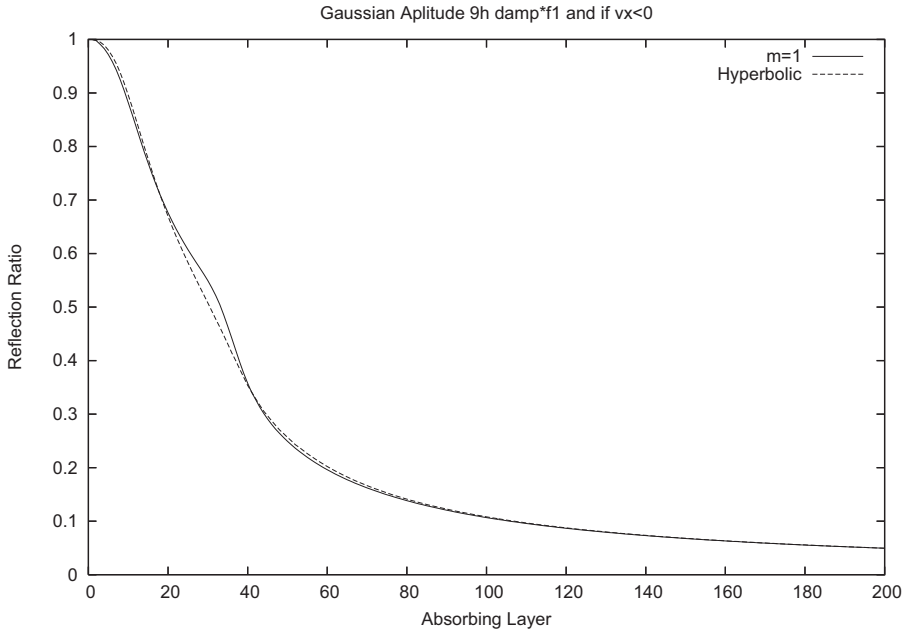

Fig. 6. Reflection ratio versus the thickness of the absorbing layer for two different distributions of the absorption coefficient (solid line $m=1$ and dashed line hyperbolic). With attenuation of the horizontal pressure force with a linear function f_1 within the damping zone and use of damping only if the speed of the particles (not of the wave) is negative $v_x<0$ in the absorbing layer. The parameters are identical to those used in Fig. 1.

computed following the Modave et al. (2010) formula, i.e. the ratio of the errors

$$R=\sqrt{\frac{E_{lay,\infty}}{E_{refl,\infty}}} \tag{0.18}$$

given by

$$E_{refl,\infty}(t)=\frac{1}{2}g\int(H_{refl}-H_{\infty})^2dx+\frac{1}{2}H\int(v_{refl}-v_{\infty})^2dx \tag{0.19}$$

where the label ∞ identifies the values obtained with an extremely far right edge, i.e. no boundary condition (BC), the label *lay* refers to the quantities evaluated with a specific absorbing layer, the label *refl* refers to the quantities evaluated with a totally reflecting BC. Obviously the integrals have been replaced by a sum over the particles. Essentially we are measuring the differences of the flow variables and then we compute the relative energy, i.e. we are not computing the differences of the energies contained in the integration domain.[1] The time evolution of the wave height, for a 100 m amplitude layer with a hyperbolic damping function (Section 3.3.), typically appears as depicted in Fig. 2, where each profile is taken at time intervals of $\Delta t=7.4$ s.

3.3. 1D simulation results

Fig. 3 shows the reflection ratio for the various damping functions obtained with different values of the exponent m and the hyperbolic function. For small layers the best performances are obtained for the linear and the hyperbolic functions. However we focused our study on the hyperbolic function since it shows better results when we add the *ad hoc* physical switches.

Fig. 4 shows the reflection ratio as a function of the thickness of the absorbing layer for two different functions of the absorption (left panel: $m=1$, right panel: hyperbolic), i.e. we compare functions which are more efficient when it is the small absorbing layer case. The solid line identifies the case with the use of the function without any switch, and we call it the *clean* function; the dashed line identifies the results obtained with the same clean function with the addition of a further tool: attenuation of the pressure force with a linear function f_1. The dotted line identifies the case of attenuation of the pressure force with a quadratic function f_2. The best results are obtained with the dashed line, i.e. linear cutting function.

Fig. 5 shows the reflection ratio results obtained by adding the velocity switch. The best results are displayed with a dotted line, corresponding to a damping with the use of the cutting function f_1 and with the simultaneous use of unidirectional friction, i.e. use the damping friction σ only if $v_x<0$, so that the damping acts only if the speed of the particles (not of the wave) is negative.

Fig. 6 compares the best results obtained with the $m=1$ and the hyperbolic damping function using both the switches f_1 and $\sigma\neq 0$ *if* $v_x<0$. The hyperbolic function works only moderately better, but in the 2D case we find a much better performance and therefore we focus on that function.

3.4. 1D simulation conclusion

Resuming the 1D case, we may say that the best results have been obtained with the hyperbolic damping function $\sigma_0[(x-x_0)/((x_0+L)-x)]$, plus two further treatments: the decrease of the horizontal pressure force with a linear function f_1 only in the damping layer and the use of damping only if the speed of the particles in the absorbing layer is negative $v_x<0$.

We have to comment that, since we are using a Lagrangian approach (the particles are free to move), we added in the denominator an extra softening term $0.5h$ to avoid division by zero if a particle reaches the left edge $\sigma=\sigma_0[(x-x_0)/((x_0+L)-x+0.5h)]$. So hereafter we report only the results obtained with the hyperbolic damping function.

Finally Fig. 7 shows the values of the reflection coefficient versus the amplitude of the damping layer for different widths of

[1] That would be $(1/2)g\int(H_l^2-H_\infty^2)dx+(1/2)H\int(v_l^2-v_\infty^2)dx$.

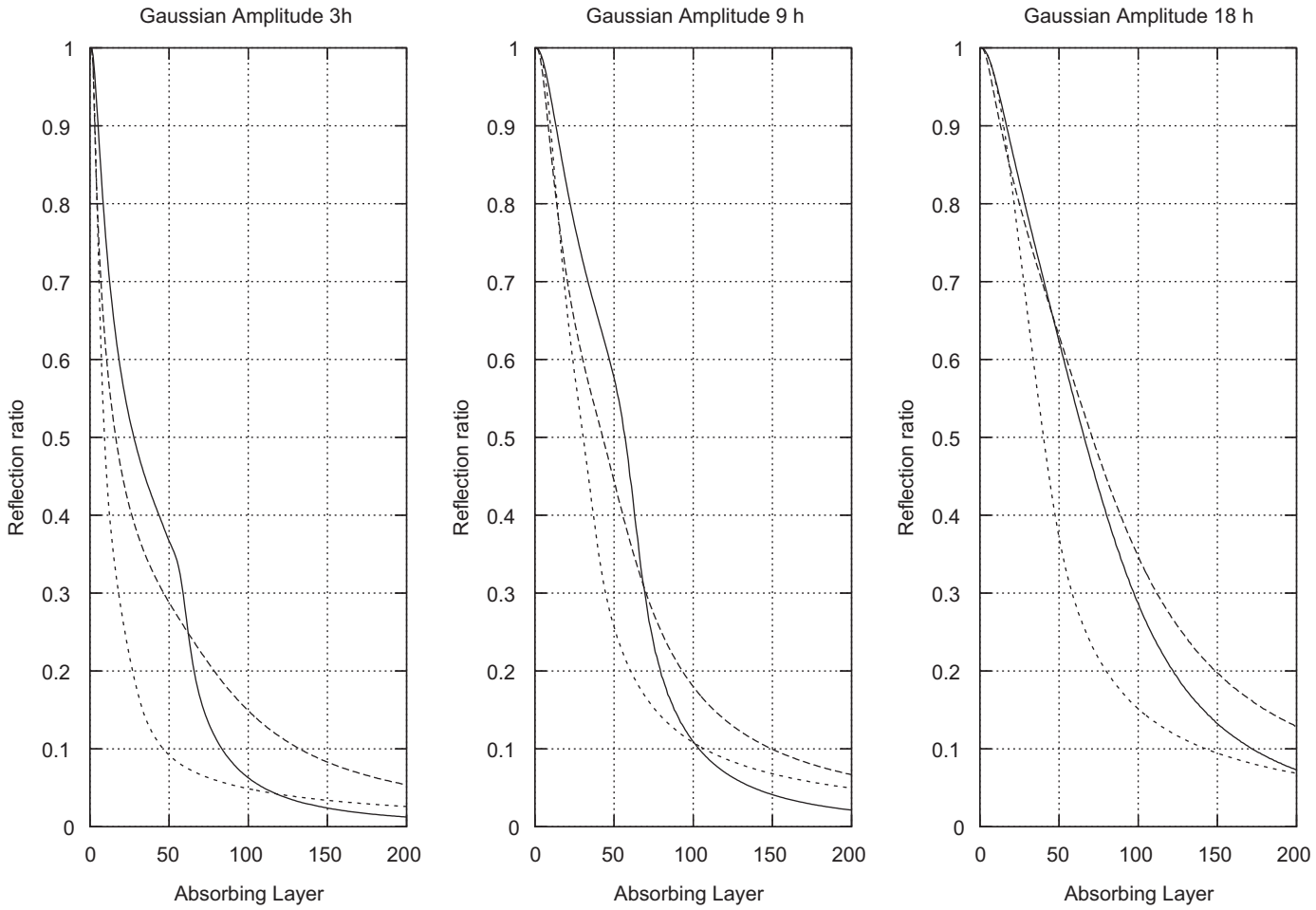

Fig. 7. Reflection coefficients for increasing length of the damping layer. The results displayed with the solid, dashed and dotted lines are obtained with the clean hyperbolic damping function, f_1 pressure factor, f_1 and speed switch respectively.

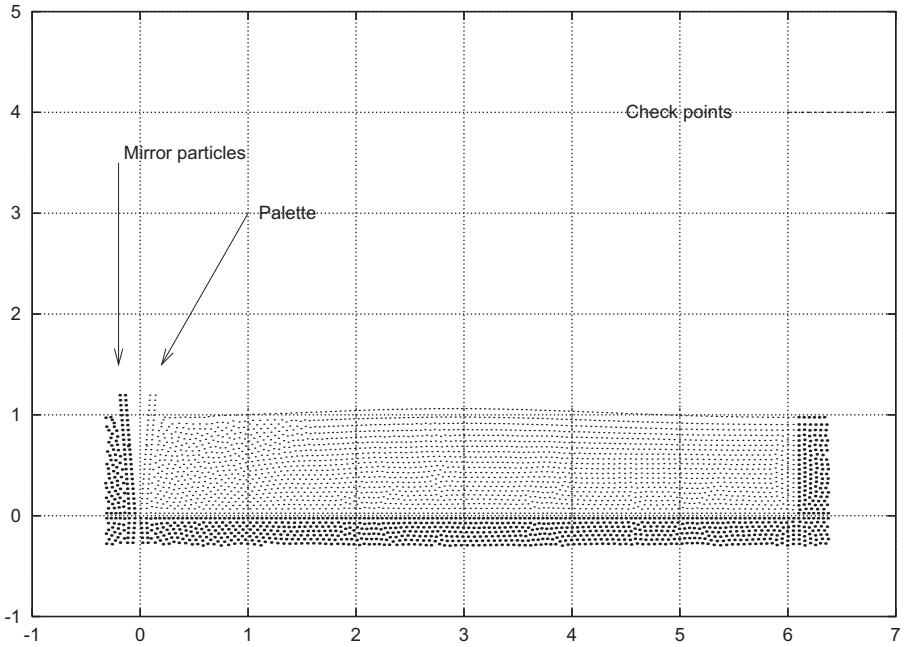

Fig. 8. Tank with wavemaker and mirror particles, with no layer added.

the Gaussian pulse. It shows the predictable result that the increase of the amplitude requires a larger damping layer to obtain the same reflection ratio.

4. Waves in tank: 2D case

In this case we study the wavy motion produced by a wave maker palette in a water tank. The dynamics is truly two dimensional. To simulate incompressible water waves we use the weakly compressible approximation (Monaghan, 2005), which consists essentially in the use of a sound speed an order of magnitude larger than the maximum typical speed of the water, and we chose $c_s=20v_{typ}$, where $v_{typ}=\sqrt{gH}$. Note that, as suggested by Madsen and Shaffer (2006), here we use as typical speed the wave speed and not the very small fluid speed. The governing equations are the previous ones, but with the equation of state given by the Tait equation:

$$P=\frac{\rho_0 c_s^2}{\gamma}\left[\left(\frac{\rho}{\rho_0}\right)^{\gamma}-1\right] \tag{0.20}$$

with $\gamma=7$.

The wavemaker is placed at the left side of the rectangular tank. A damping layer is added in the right side. Check points of the water level are defined at regular space intervals. The setup is shown in Fig. 8.

The aim is to produce, in the finite tank of length X, a motion, unaffected by the right boundary, i.e. equal to the one obtained in the same zone but in an infinite tank.

We added the same source terms used for the 1D case to the equations of motion and continuity, taking into account the dimensionality of the problem, and we added a term $Q_\alpha=-\sigma_\alpha(v_\alpha-v_{0_\alpha})$ to each component of the momentum equation. In this study $v_{0_\alpha}=0$.

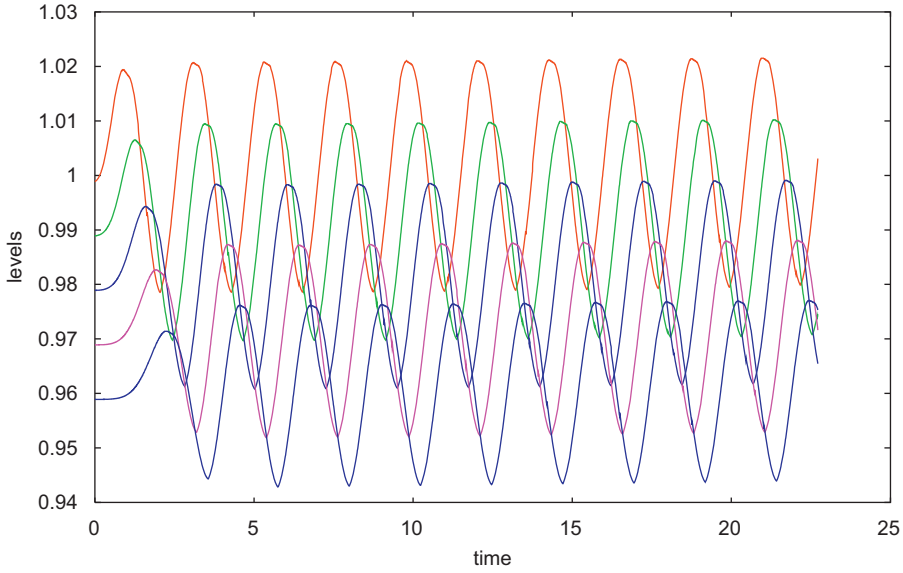

Fig. 9. Levels at $x=1, 2, 3, 4, 5$ m in an "infinite tank".

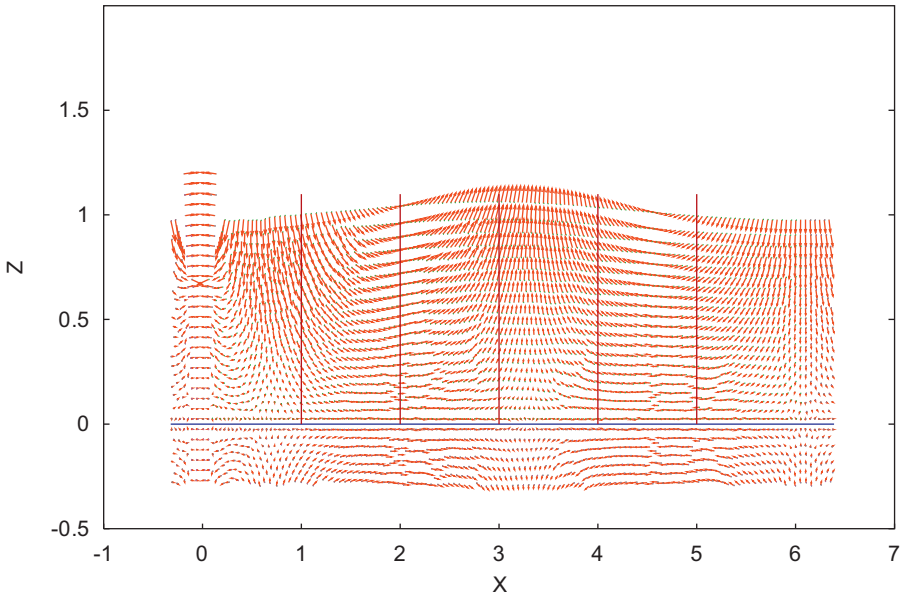

Fig. 10. Velocity field of the water in the resonant case, with no damping layer.

Also we explored some "*ad hoc*" terms, guided by the 1D experience and physical intuition:

- a switch on the damping triggered by the speeds v_x and/or v_y,
- the use of cutting functions to reduce the horizontal component of the force due to the pressure.

We examined the case of a continuous periodic wave and that of a wave generated by a single sinusoidal oscillation.

4.1. Continuous periodic wave

We made a tank of length $X=6.061$ meters and height 1 m. The particles have an intrinsic width $h=0.1$ and are placed at a regular spacing $\Delta l=0.05$ in X and Z. The number of particles in the tank is $N=2570$ (wavemaker included). The boundaries are made with mirror particles procedure. The wavemaker oscillates with a period $P=2.23$ s and with an angle amplitude of 5°. With these values the water in the tanks enters in a resonant state. Fig. 9 reports the levels of the water column, measured at five different positions (at $x=1$, 2, 3, 4, 5 m) along the tank, versus elapsed time, in the case of a very long "infinite" tank.

The levels are vertically shifted for clarity. It is clear that the waves propagate without disturbances.

Fig. 10 shows the velocity field of the tank in resonant condition, with the wavemaker and the mirror points.

Fig. 11 shows the levels for the resonant tank. The levels are shifted in the Z coordinate by a small amount $dz=0.01$ for clarity.

It is clear that the oscillations are larger and increasing with time.

In Fig. 12 we show the resulting levels when a damping layer of extension $L=6.061$ m is added. That is, we are using a full simulation domain $X=12.122$ m. In all these tests the hyperbolic function $\sigma=\sigma_0[(x-x_0)/((x_0+L)-x+0.5h)]$ is adopted. The coefficient σ_0 has the dimension of 1/time and we chose its value as σ_0-v_{ref}/L. For this study the reference speed has been chosen equal to the sound speed: $v_{ref}=c_{sound}$ (case with the label *M0*).

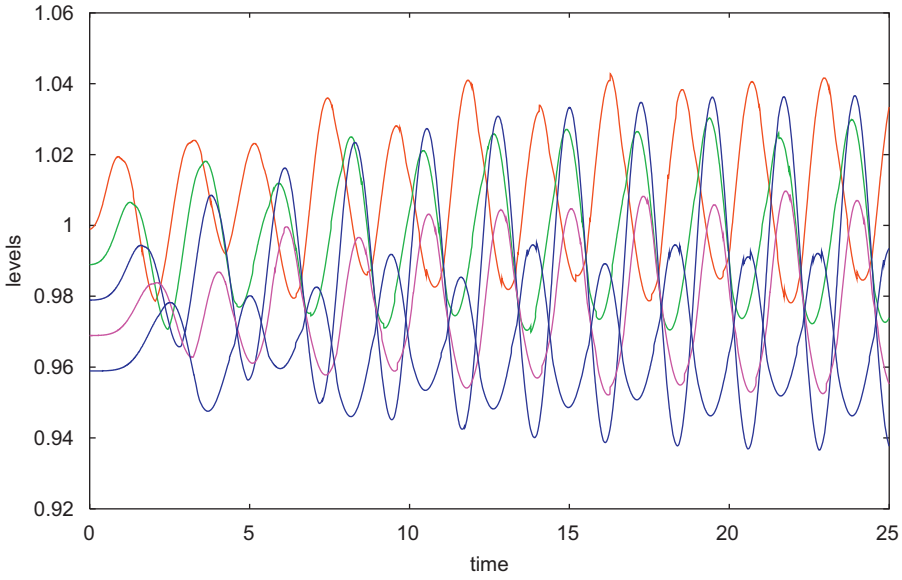

Fig. 11. Water levels in the resonant case.

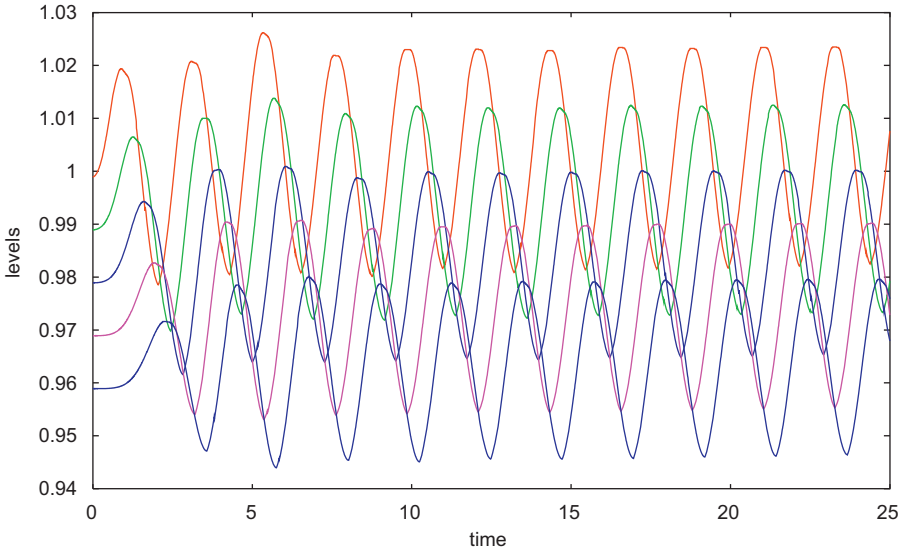

Fig. 12. Water levels for the case *M0*: plain hyperbolic absorption function.

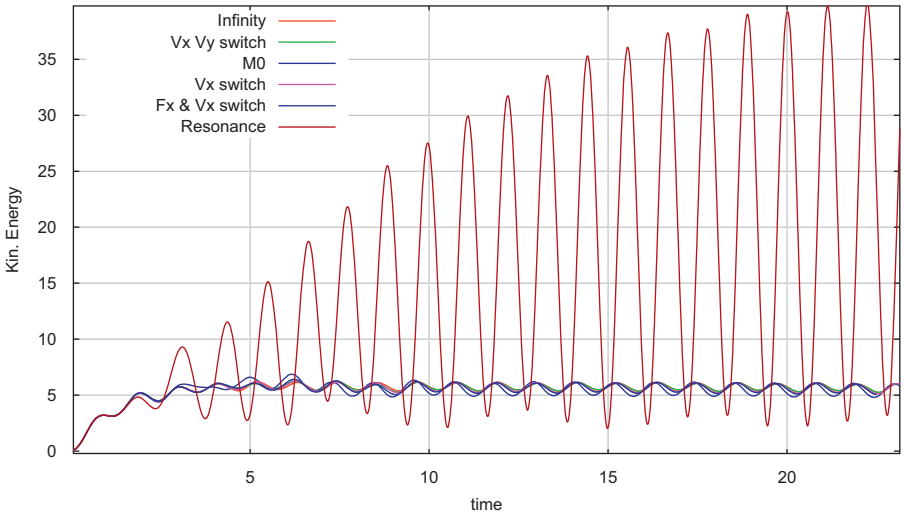

Fig. 13. Kinetic energy versus time for resonance and for boundary layer with switches.

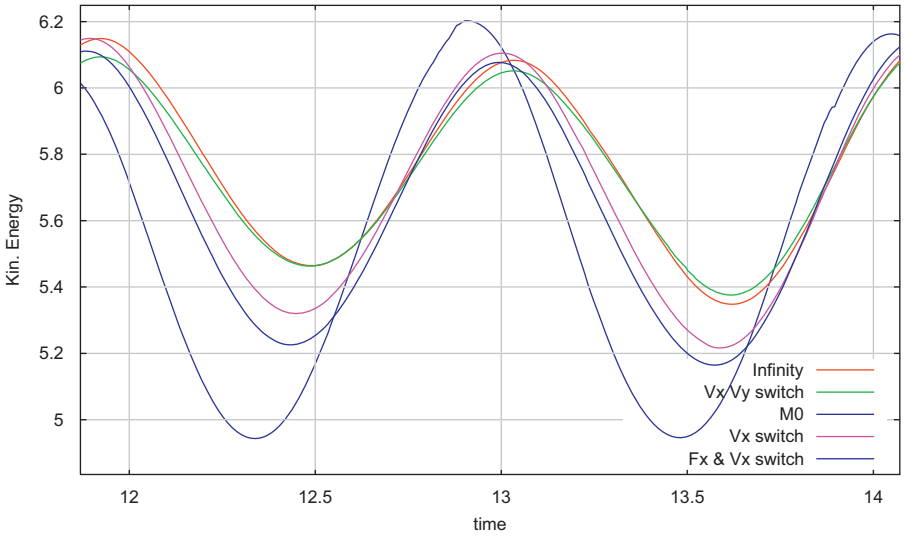

Fig. 14. Zoom on the kinetic energy versus time.

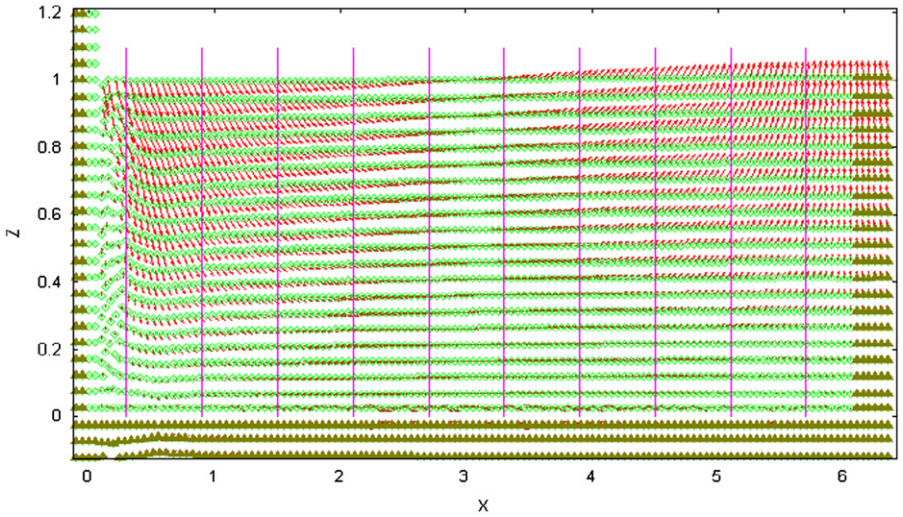

Fig. 15. The particles configuration and their speed (enlarged by a factor 2.5) for the water in a reflecting tank.

It is clear that the wave profiles are very similar to the ones of the *infinity* case.

The kinetic energy content can be used as an indicator of the similarity of the flows. Fig. 13 shows the kinetic energy of the water (computed excluding the damping layer contribution) versus time for various cases. The increase of the energy in the resonant condition, the steady oscillating energy for the *infinity* case, together with the very close values obtained with different damping layer cases are clearly shown.

If we zoom Fig. 13, on the values of the kinetic energy, we obtain Fig. 14 and find some discrepancies between the *infinite* case and the *M0* one.

We made the same simulation to test the following set of switches:

"V_x V_y": the damping function works only if $v_x<0$ and $v_y<0$,

"V_x": the damping function works only if $v_x<0$,

"F_x and V_x": the damping function works only if $f_x<0$ and $v_x<0$.

If we look at the kinetic energy we find that performances better than *M0* are obtained with each of the switch options mentioned, since for *M0* the kinetic energy has oscillations larger than the ones of the *infinity* case. Qualitatively, the best result seems to be obtained with the simple "V_x" switch. However further investigations should be carried out to produce a numerical estimate.

4.2. Sinusoidal single impulse wave

We made also simulation of a single impulsive sinusoidal wave. In the same tank, the wavemaker makes a single oscillation with the same angular amplitude and period of the previous simulation. In this case it is easy to see the effects of the reflected

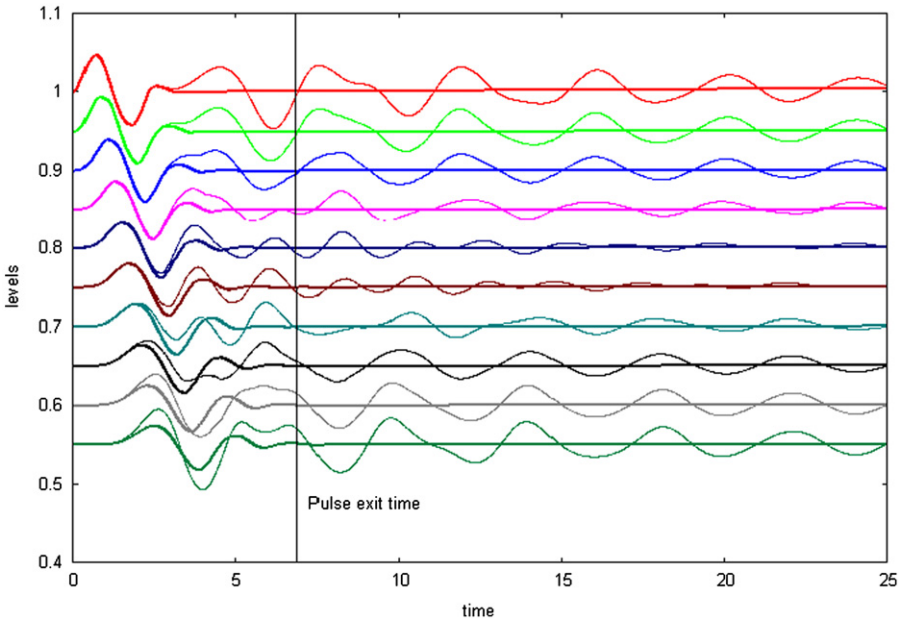

Fig. 16. Ten levels for reflecting BC tank compared to the levels of the *infinity* case.

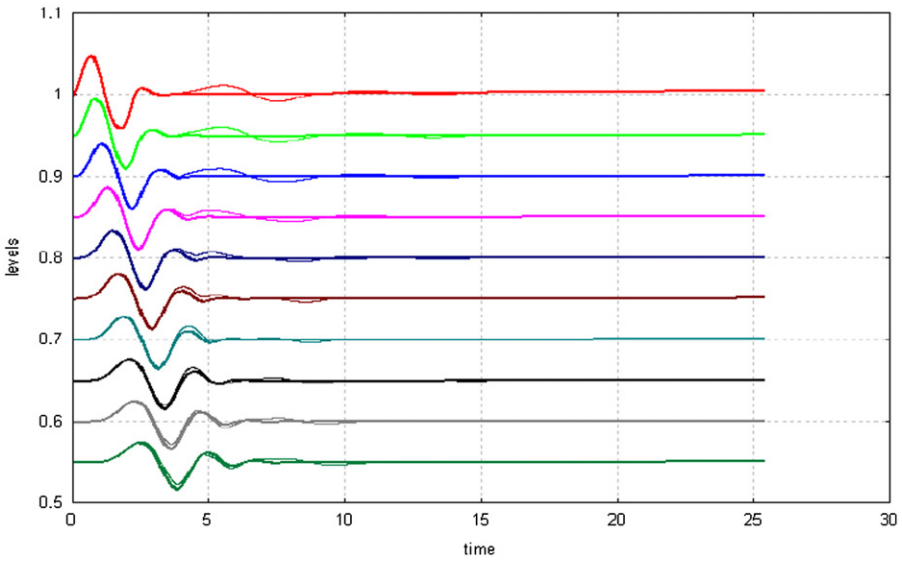

Fig. 17. Comparison of levels obtained with the *M0* prescription and the *infinity* case.

wave. To have a detailed information, in this case we chose ten elevation level points located at intervals of 0.6 m, starting from 0.3 m from the left side. Fig. 15 shows the particles and their velocity field for the water in the tank at *time* $t=25$ s; this is the configuration without any damping layer, i.e. clean reflection conditions at the right side. The vertical lines identify the points of level measurement. The particles distribution and the speed arrows show that the water level is still oscillating.

Fig. 16 shows in the same panel the levels when the tank has a simple reflecting boundary on the right side; the levels obtained for the *infinite* tank (the thicker and straighter horizontal lines) are also plotted. It is obviously clear that oscillations are present even after the long time the pulse had to be outside the tank.

In Fig. 17 are shown the levels obtained with the *M0* prescription compared with the *infinity* case.

In Fig. 18 the *M0* levels are plotted together with the ones obtained with the "V_x V_y" switch. The *M0* lines show a small bump around time $t=5$–6 s, while the thick lines are more straight; they correspond to the use of the "V_x V_y" switch.

We studied also the same two problems using smaller damping layers. The results are similar to the one presented here with the obvious difference that the damping effects diminish as the layer thickness decreases. We show the results of the single sinusoidal impulse. Fig. 19 shows the kinetic energy of the tank versus time when the length of the damping zone is $L=6.06$.

Fig. 20 shows the kinetic energy of the water in the tank for a shorter damping layer $L=3.03$ m. We also tested the use of cutting functions, but the improvements are very small to be appreciated in the figure. From Fig. 20 it is clear that the reducing action of the residual oscillations is due to the velocity switch when added to the plain damping function.

Fig. 21 shows a zoom of Fig. 20, to show clearly the different effects of the damping criteria. It shows that for the 2D problem the cutting function improves the results over the plain damping, but it is not better than the simple velocity switch. The joint action of the velocity switch and of the cutting function does not improve the result.

5. Conclusion

The use of a damping layer is successful in avoiding boundary reflections into the computational domain. An obvious requirement is that the absorbing layer must be greater than or equal to the maximum significant wavelength produced by the physical

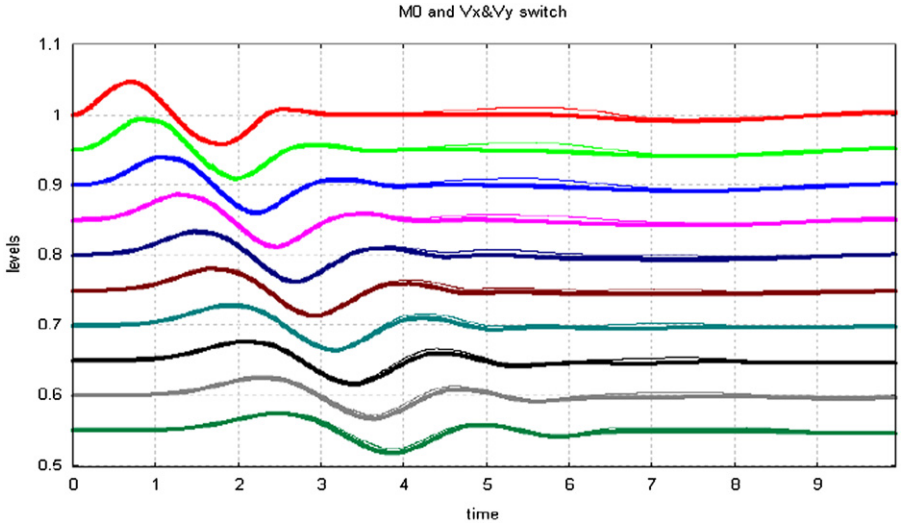

Fig. 18. Comparison of levels obtained with *M0* and with the switches *Vx* and *Vy* (thick lines).

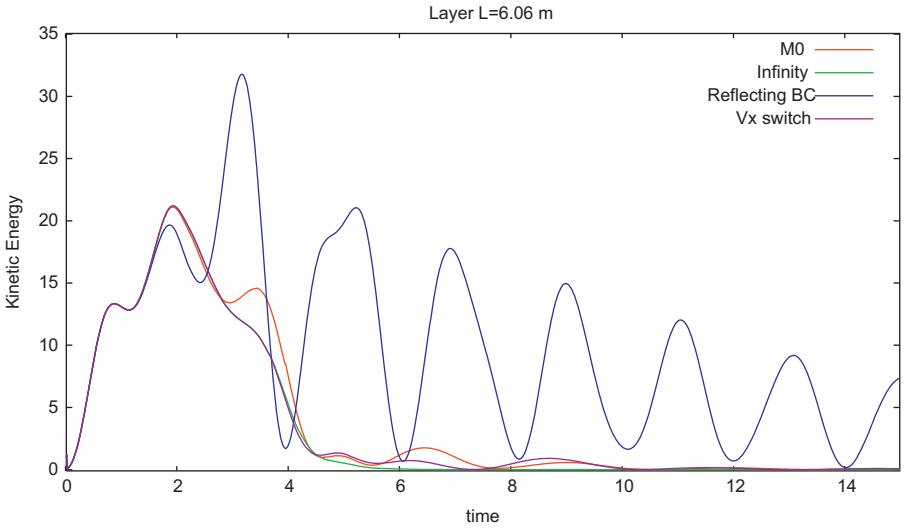

Fig. 19. Kinetic energy for different damping actions in the case of a 6.06 m large damping zone.

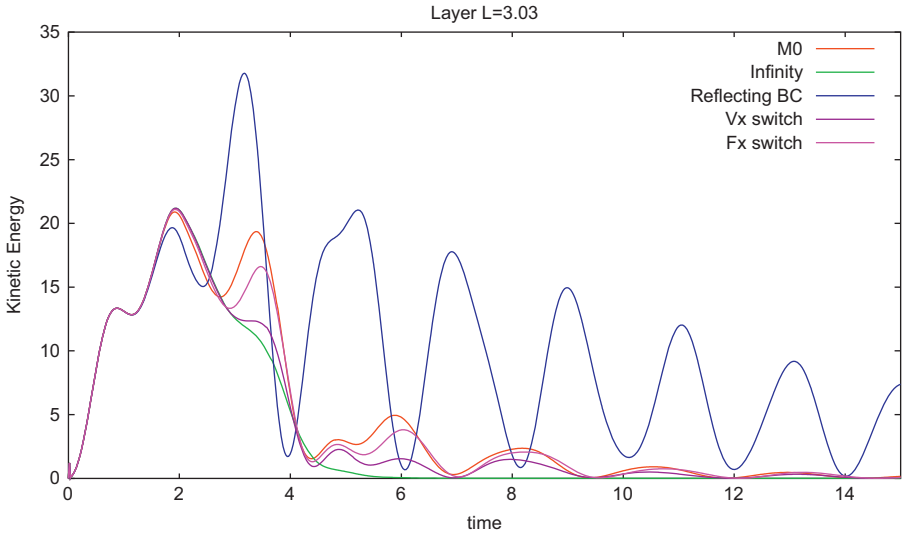

Fig. 20. Kinetic energy of the water in the case of damping layer $L=3.03$ m.

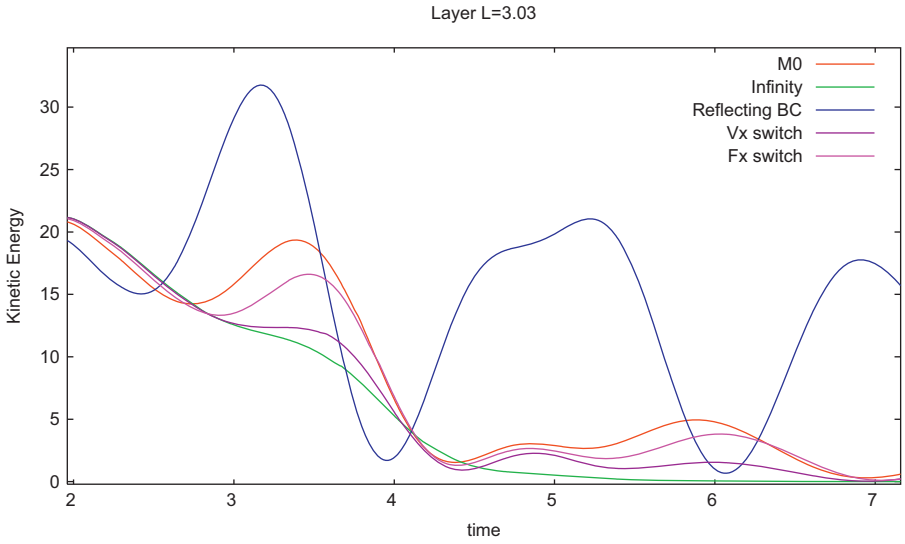

Fig. 21. Zoom of Fig. 20 to show better results of the different damping algorithms.

simulation. Both in the 1D and 2D cases the basic procedure can be improved by the use of appropriate switches. A simple and efficient switch is the one that makes the damping operate only for negative speeds, i.e. $v_x<0$. The switch that reduces the horizontal component of the force, F_x, is efficient in 1D, but not so much for the 2D problem we studied. Further work is in progress to make a quantitative evaluation of the 2D simulations and verify the affordability of the method in the case of highly compressible fluid dynamics.

Acknowledgments

R. Grammauta acknowledges CRRSN for a six months grant exploited for this study.

References

Antuono, M., Colagrossi, A., Marrone, S., Lugni, C., 2011. Comput. Phys. Commun. 182 (4), 866–877.

Berenger, J.P., 1994. A perfectly matched layer for the absorption of electromagnetic waves. J. Comp. Phys. 114, 185–200.

Colagrossi, A., Landrini, M., 2003. Numerical simulation of interfacial flows by smoothed particle hydrodynamics. J. Comp. Phys. 191, 448–475.

De Leffe, M., Le Touzé, D., Alessandrini, B., 2010. SPH modeling of shallow-water coastal flows. J. Hydraul. Res. 48 (2010), 118–125 (Extra issue).

Engquist, B., Majda, A., 1977. Absorbing boundary conditions for numerical simulation of waves. Proc. Natl. Acad. Sci. USA 74 (5), 1765–1766.

Lastiwka, M., Basa, M., Quinlan, N.J., 2009. Permeable and non-reflecting boundary conditions in SPH. Int. J. Numer. Methods Fluids 61, 709–724.

Lin, D.K., Li, X.D., Hu, Q., 2011. Absorbing boundary condition for nonlinear Euler equations in primitive variables based on the Perfectly Matched Layer technique. Comput. Fluids 40, 333–337.

Madsen, P.A., Shaffer, H.A., 2006. A discussion of artificial compressibility. Coastal Eng. J. 53, 93–98.

Modave, A., Deleersnijder, É., Delhez, J.M., 2010. On the parameters of absorbing layers for shallow water models. Ocean Dyn. 60, 65–79.

Monaghan, J.J., 2005. Rep. Prog. Phys. 68, 1703–1759.

Monaghan, J.J., 2006. Mont. Not. R. Astron. Soc. 365, 199–213.

Poinsot, T.J., Lele, S.K., 1992. Boundary conditions for direct simulations of compressible viscous flows. J. Comp. Phys. 101, 104–129.

Riadh, Ata, Azzedine, Soulaimani, 2005. A stabilized SPH method for inviscid shallow water flows. Int. J. Numer. Methods Fluids 47, 139–159.

Vacondio, R., Rogers, B., Stansby, P., Mignosa, P., 2012. SPH modeling of shallow flow with open boundaries for practical flood simulation. J. Hydraul. Eng. 138 (6), 530–541.